Journal of the Korean Nuclear Society
Volume 28, Number 4, pp. 379~389, August 1996

Interfacial Wave Characteristics for Countercurrent Stratified Air-Water Flow in a Horizontal Pipe

Heung June Chung, Se Young Chun, and Moon Ki Chung
Korea Atomic Energy Research Institue
150 Dukjin-dong, Yusong-ku, Taejon 305-353, Korea

Hee Cheon No
Korea Advanced Institute of Science and Technology
Department of Nuclear Engineering
373-1 Kusong-dong, Yusong-gu, Taejon 305-701, Korea

(Received January 10, 1996)

Abstract

To experimentally investigate the several wave patterns for the horizontal countercurrent stratified air-water flow, a series of systematic experimental studies have been performed. The experiments are carried out in a horizontal pipe with 4m in length and 102mm in inner diameter. The water and air superficial velocities vary from 0.0004 to 0.0204 and from 0 to 6m/s, respectively. The instantaneous water thickness is measured by parallel-wire conductance probes, and the wave field is recorded by high speed video camera. Also, to evaluate the wave effects on interfacial friction factor, the pressure drop is measured. Statistical data analysis is accomplished in order to obtain the fundamental wave parameters such as wave amplitude, length and velocity, and spatial growth factor. By using these statistical parameters, the wave regime boundaries can be verified.

1. Introduction

A stratified two-phase flow pattern is characterized by liquid moving along the bottom of the horizontal flow channel with gas above it. In the stratified flow, the countercurrent flow patterns have many engineering applications such as in the tubular reflux condenser, boiler, refrigerator tubes, oil and natural gas pipelines and safety related problems of the pressurized water reactors(PWRs).

Many studies have been carried out both experimentally and analytically on cocurrent flow in horizontal pipes [1~3]. The countercurrent flow in vertical flow channel also has been studied by numerous investigators [4~6].

For horizontal countercurrent flow, most of studies have been focused on explicating of transition mechanism from stratified to slug flow [7, 8]. Therefore, basic informations for understanding the interfacial structure and dynamics of the countercurrent stratified flow in horizontal geometries are not sufficient. Subsequently systematic studies on wave characteristics of horizontal countercurrent two-phase flow are needed. And in the literature discussed above, transitions between the various subregions have been defined by visual observations. Such visual observations

apparently cause disagreement amongst researchers.

The objectives of the present study are to experimentally identify the wave regime transition in horizontal countercurrent air-water flow. Then, the transition boundaries between wave regimes are to be quantified by statistical data analysis. Finally, the effects of wave regimes on pressure drop characteristics, which is a key parameter in the analysis of two-phase flow, are to be analyzed.

2. Experimental Setup and Method

A schematic diagram of the experimental setup is shown in Fig. 1. It consists of a test section, an air supply system and a water supply system. The dimension of the test section is 4 m in length and 102mm in inside diameter. The test section is made of acrylic tube for visual observation and high speed video imaging of the wave field. Pressure taps to measure the air pressure drop are installed, and three parallel-wire conductance probes to measure instantaneous water thickness are installed at L/D = 6 .7, 24.2, and 24.3, respectively, from the air inlet. Filtered water and air are used as working fluids. The water is pumped by a centrifugal pump from the wat er storage tank to the test section. Water flow rate is measured by three precision rotameters.

The air to the test section is supplied by the central air supply system in Korea Atomic Energy Research Institute. The maximum air pressure is 7 bar and the volumetric flow rate is regulated by a pressure regulator installed in the air supply line. Also a fine mesh is installed at the air line of the test section to enhance the flow quality. And the volumetric air flow rate is measured by precision rotameters installed in parallel at the air supply line.

The air pressure drop between pressure taps is measured by using a micromanometer which has 99mm H_2O in full scale and a high speed video cam era system is used to record the wave field. The cam era is operated by 250 frames/s.

The parallel-wire conductance probe for present

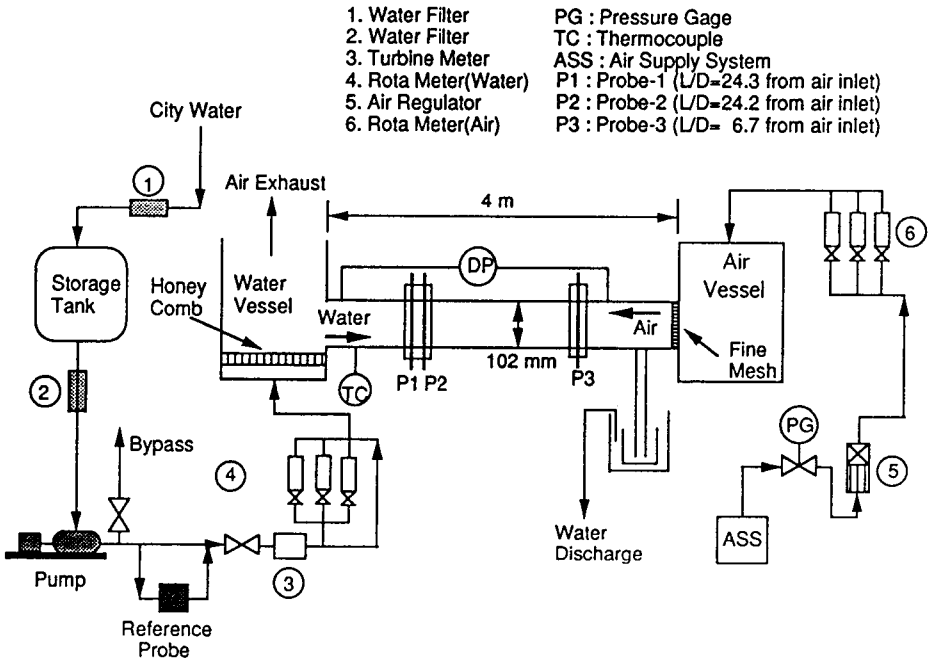

Fig. 1. Schematic Diagram of the Horizontal Air-Water Loop

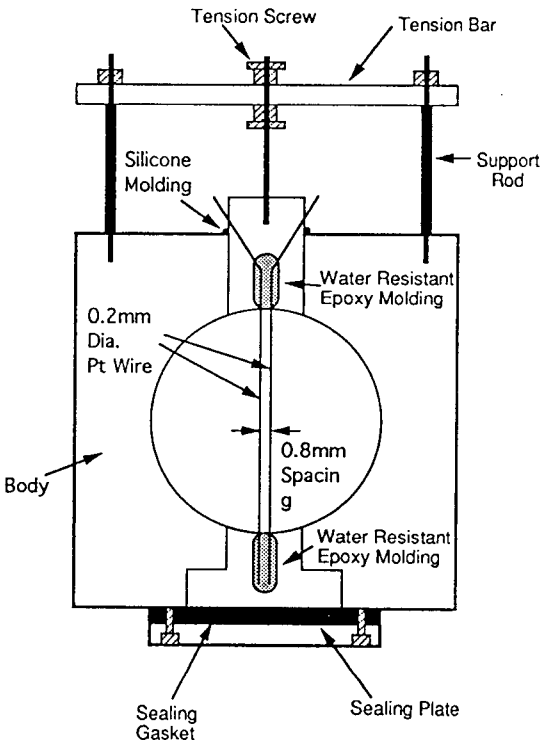

Fig. 2. Configuration of Parallel-Wire Conductance Probe

study was constructed based on the results of Koskie et al. [9].

The configuration of the parallel-wire conductance probe for the present study is shown in Fig. 2. The probe consists of two parallel 0.2mm diameter platinum wires which are spaced by 0.8mm center spacing. To eliminate the measurement uncertainty from low frequency vibration and non-parallelism between wires, a sufficient tension is maintained by the tension screw. To measure the propagating wave properties such as wave velocity and wave length, two identical probes 15mm apart from each other are arranged perpendicular to the flow direction. Calibration and performance test were conducted for the present parallel-wire conductance probes [10].

The experiments were carried out under quasi-steady state and fully developed flow conditions. By changing the air and water flow, a wide range of stratified flow pattern region was covered. The water superficial velocity varied from 0.0004 to 0.0204 m/s and the air superficial velocity ranged from 0 to about 6m/s. Data acquisition and fast Fourier transform condition are illustrated in Table 1.

Table 1. Data Acquisition and FFT Condition

Parameters	Value
Sampling Frequency	204.8 Hz
Total Number of Data per Channel	65536
Total Length of Sample Record	320 sec
FFT Size	512
Number of Ensemble Averaging	128

3. Statistical Data Analysis

Basic statistical properties can be obtained by applying the fast Fourier transform(FFT) method to the instantaneous water thickness signals. For a single sample record Power Spectral Density Function can be obtained. From two sample records Cross-Correlation Function which is used to calculate the wave velocity, Cross-Spectral Density Function which is used to calculate the wave length and Transfer Function can be derived. The FFT techniques are described in detail by Bendat and Piersol [11].

The dynamic characteristics of the linear system can be described by a transfer function(TFN). The magnitude of TFN, $|H(f)|$, is called the system gain factor, and it means the ratio of output amplitude to input amplitude. Therefore TFN can be used to evaluate the degree of spatial damping or growing of the propagating interfacial waves.

From normal mode formulation of waves, the interfacial wave signals can be described as

$$v_j = v_{oj} \exp [i k (z_j - c t)] , \quad (1)$$

where c is the complex speed of disturbances. In Eq. (1), for a spatially growing normal mode, k is complex i.e., $k = k_R(f) + ik_I(f)$ but the wave frequency $\omega = kc$ is real. The flow is unstable with respect to spat-

ial disturbance if $k_i < 0$. k_i, which is called "growth rate", can be determined from system gain factor as

$$k_i(f) = -\frac{1}{\Delta z} \ln[\,|\,H(f)\,|\,] \quad (2)$$

In the present study, "spatial growth factor(SGF)" is defined as the value of k_i at the most coherent frequency, since it can be treated as the most unstable one which will dominantly propagate and be more easily amplified than those with other frequency components.

4. Pressure Drop Characteristics

Consider the horizontal countercurrent stratified air-water flow model shown in Fig. 3, and assume that the flow is fully developed. Then, the momentum balance for gas phase gives

$$-A_g \left(\frac{dp}{dx}\right) = \tau_{wg} S_g + \tau_i S_i \quad (3)$$

As shown in Fig. 3, Eq.(3) represents a balance between the pressure forces on the gas space and the resisting stresses at the gas-solid wall boundary, τ_{wg}, and at the gas-liquid interface, τ_i.

Taitel and Dukler[12] represented the stresses in terms of the friction factors

$$\tau_{wg} = \frac{1}{2} f_g \rho_g V_g^2, \quad (4)$$

$$\tau_i = \frac{1}{2} f_i \rho_g V_g^2. \quad (5)$$

Using the pressure drop Eq.(3) can be rewritten as

$$A_g \left(\frac{\Delta P}{L}\right) = \tau_{wg} S_g + \tau_i S_i. \quad (6)$$

Substituting Eqs.(4) and (5) into Eq.(6) and solving for f_i gives

$$f_i = \frac{1}{S_i V_g^2} \left(\frac{2 A_g \Delta P}{\rho_g L} - f_g S_g V_g^2\right). \quad (7)$$

The gas-to-wall friction factor in Eq.(7) is determined from the experiment conducted under the conditions of single phase air and the definition of the skin friction factor, C_f:

$$C_f = 4 f_g = \frac{\Delta P}{\left(\frac{L}{D}\right)\frac{(\rho_g V_g^2)}{2}} \quad (8)$$

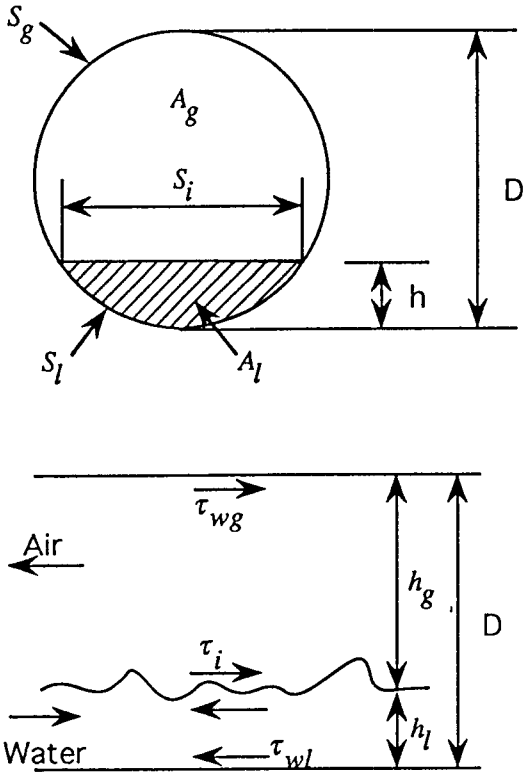

Fig. 3. Model Used for Analysis of Interfacial Friction Factor

5. Results and Discussion

5.1. Interfacial Wave Regimes

It is of importance first to describe the wave field obtained from the parallel-wire conductance probe and a high speed video camera. Figure 4 shows the typical time recordings of interface for the liquid superficial velocity $j_f = 0.0004 m/s$ and the corresponding photographic views obtained from high speed camera are arranged in Fig. 5.

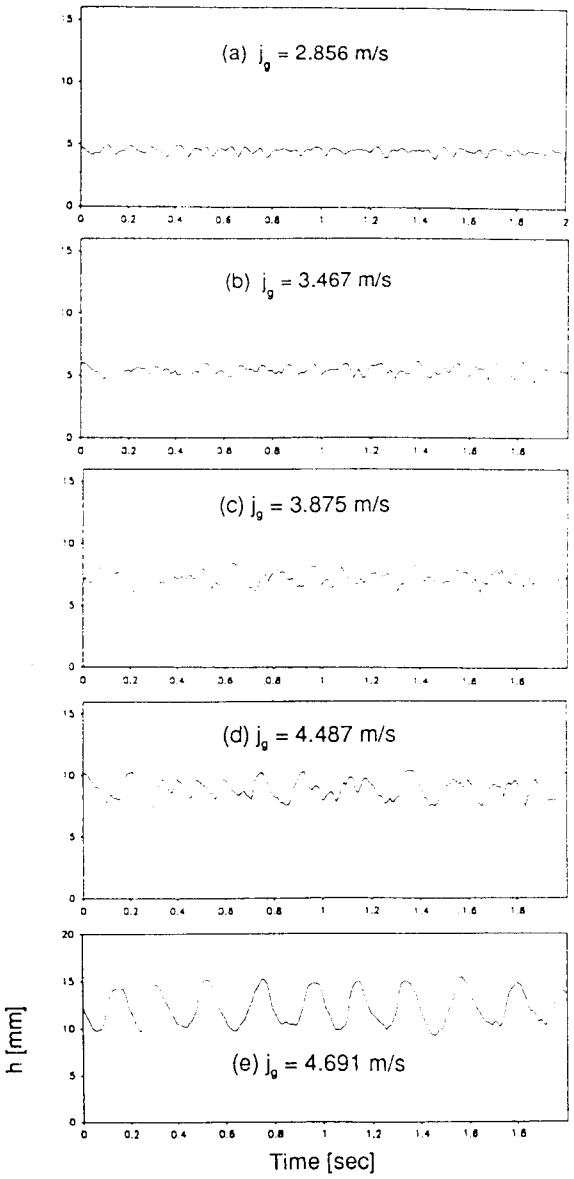

Fig. 4. Typical Time Recordings of Interface (j_f=0.0004 m/s)

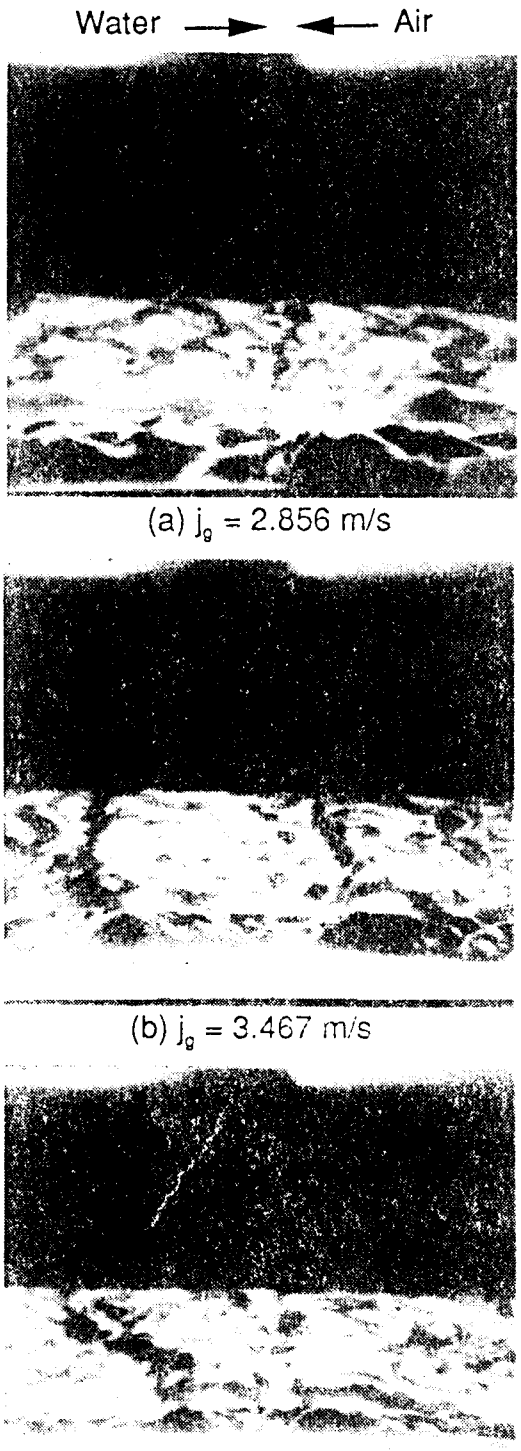

For a fixed water flow rate, the first waves observed, as increasing the air velocity, are of small amplitude pebbly waves. It is evident from Figs. 4(a) and 5(a) that these pebbly waves are irregular in amplitude and frequency. However, as the air flow rate is further increased, the transition from pebbly to 2-D

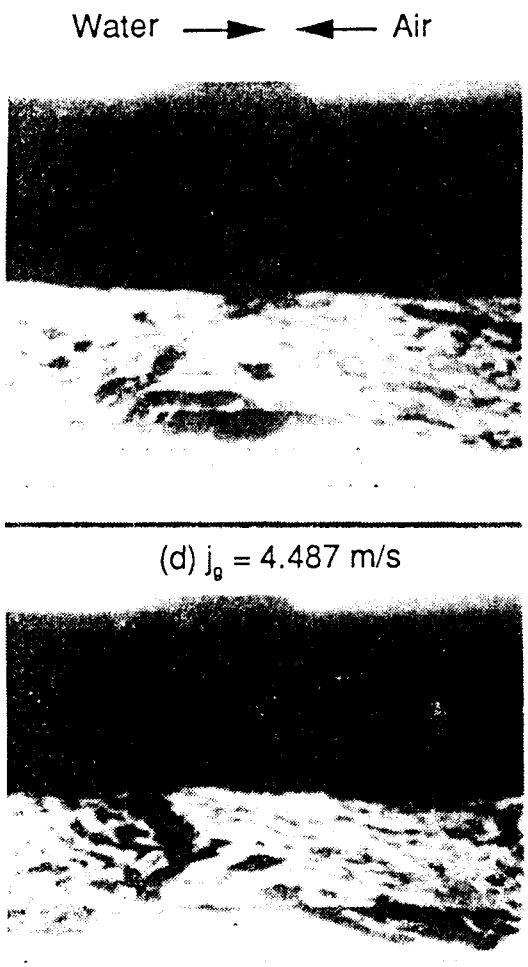

Fig. 5. Photographic Views of Wave Field (j_f=0.0004 m/s)

wave regime occurs. As can be seen from Figs. 4(b) and 5(b), these 2-D waves are irregular in amplitude and frequency, which is the same in pebbly wave regimes. However, it can be found from Fig. 5(b) that the 2-D waves span the entire channel. The important feature of these 2-D wave regimes is the existence of small capillary waves, which are almost same as the pebbly waves but different in wave length, between 2-D waves. In the 2-D wave regimes, the precursor waves leave the capillary waves and these capillary waves interact with the following 2-D waves or other ones. However, it is clear that the amplitude does not apparently increase.

Above j_g=3.9m/s, the wave interactions between 2-D waves rather than between 2-D and capillary waves occur more frequently. These 2-D wave interactions apparently increase the wave amplitude and the flow regime becomes more uneven(Figs. 4(c) and 5 (c)). As the air flow increases further the large-amplitude waves are formed on the interface(Figs. 4(d), 5 (d)). It is also interesting to note that a large increase in average water thickness occurs. It is of value to note that large-amplitude waves are asymmetric with a front side that is steeper than the backside, which is a notable feature of the large amplitude waves for the cocurrent wave data by Andritsos and Hanratty [1], Peng et al[3]. From the video imaging it is found that the large-amplitude waves are originated from two modes;continued growth and coalescence of 2-D waves. This large-amplitude regime continues at about j_g=4.7m/s, and finally reaches a flooding region (Figs. 4(e) and 5(e)). Flooding is defined as the point where the level of water in the vessel does not stagnate but increases. In the flooding region, the shape of waves appears as a large liquid lump and atomization occurs at the water inlet in the course of time.

For another water superficial velocity the transition procedures are similar to the lower water superficial velocity. The main differences are that the transition between regimes occurs at lower air velocity, and the transition into the large-amplitude region occurs in a narrower range of air superficial velocity. And for very higher range of water superficial velocities, j_f =0.0163 and 0.0204m/s, the large-amplitude waves were not observed but observed as even larger liquid lump [10].

5.2. Characterization of the Wave Field

As discussed above, the wave regime can be div-

ided into some subregions. Most previous researchers, typically Andritsos and Hanratty[1] and Peng et al. [3] have defined the subregions only by visual observations. For the present analysis the subregions are defined by using statistical method.

The amplitude, a, as a function of air superficial velocity is shown in Figs. 6 and 7. From these figures, it is evident that the wave amplitudes increase with increasing j_g for a given value of j_f, and that the slope indicating the rate of increase of wave amplitude with respect to the air superficial velocity shows some different behaviour in 2-D and large-amplitude regions.

Figure 8 shows the variation of power spectra, which indicates the dominant frequency range, for typical cases of $j_f = 0.0004$ and $0.0061 m/s$. From these figures, it can be seen that there are some peaks in pebbly and 2-D regions. This reflects that the observed wave tracings that the pebbly and 2-D waves are irregular in frequency and interaction between various frequency components waves occur as discussed above. Whereas there is a clear peak in large-amplitude region, which means that the majority of waves are dominant frequency waves and interaction between dominant waves is more abundant than between other component frequencies.

The degree of spatial growth of propagating waves can be quantified in terms of the SGF(Spatial Growth Factor) defined in Eq.(2). Figures 9 and 10 show the variation of SGF as a function of air superficial

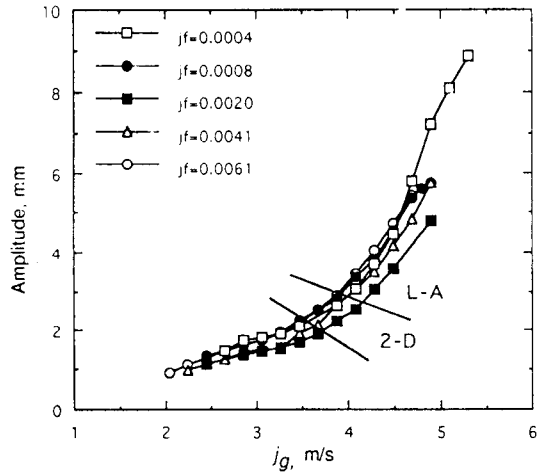

Fig. 6. Variation of Amplitude for Lower Range of j_f

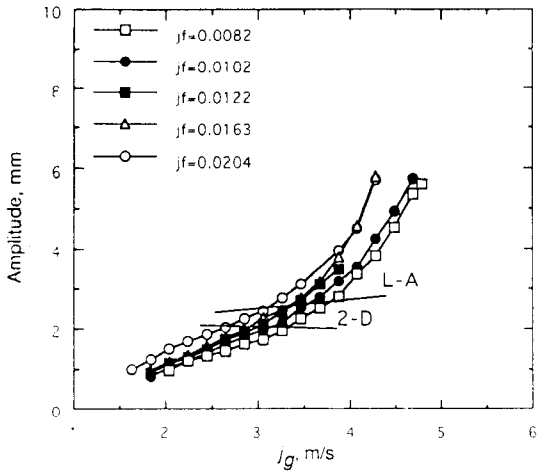

Fig. 7. Variation of Amplitude for Higher Range of j_f

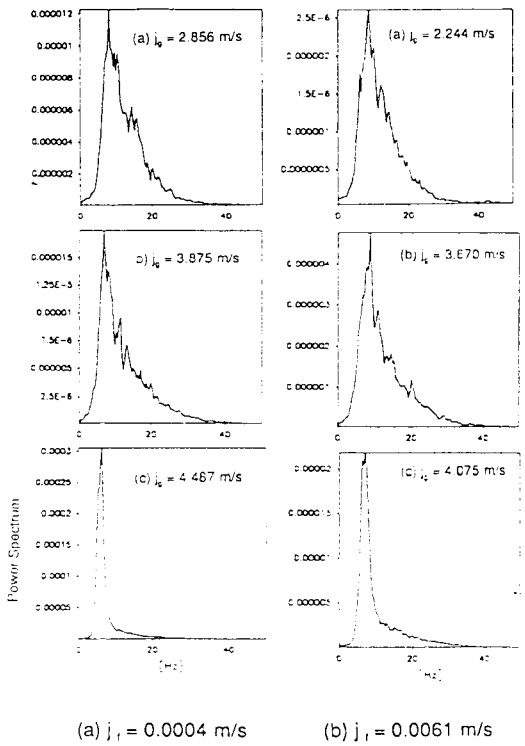

Fig. 8. Variation of Power Spectra

velocity. For the lower air superficial velocity, the values of SGF lie in growing region, which means that waves are unstable as they formed on the interface. In 2-D region, with the active wave interaction SGF gradually decreases, which is consistent with the slight increase of wave amplitude. However, with the onset of the large-amplitude waves SGF decreases drastically, which means that wave amplitude drastically increases in spatially. In Fig. 10 the quite dissimilar trends can be seen for very higher water superficial velocities, $j_f = 0.0163$ and $0.0204 m/s$. This may be associated the larger liquid lump as observed that, when the water superficial velocity is very high, the waves are evolve into larger liquid lumps rather than the large-amplitude waves. This is consistent with the result of Peng et al.[3] that for higher water Reynolds number the solitary waves were not observed. From discussion so far, it can be noted that the variation of SGF is physically consistent with the wave tracings from probes and photographic viewings from a high

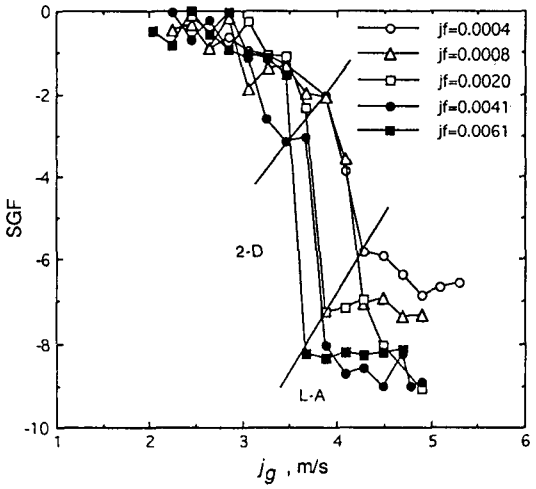

Fig. 9. Variation of Spatial Growth Factor for Lower Range of j_f

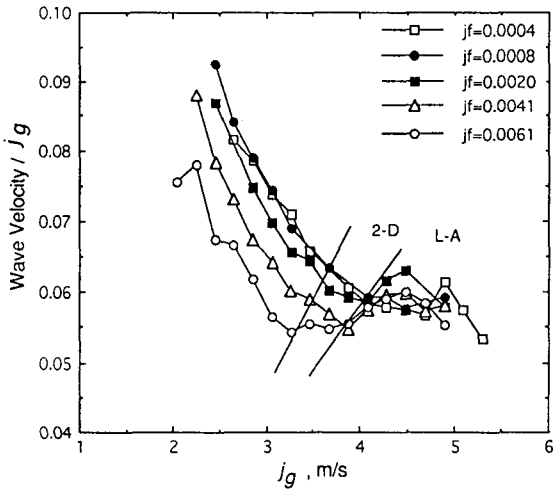

Fig. 11. Effect of j_g on Wave Velocity for Lower Range of j_f

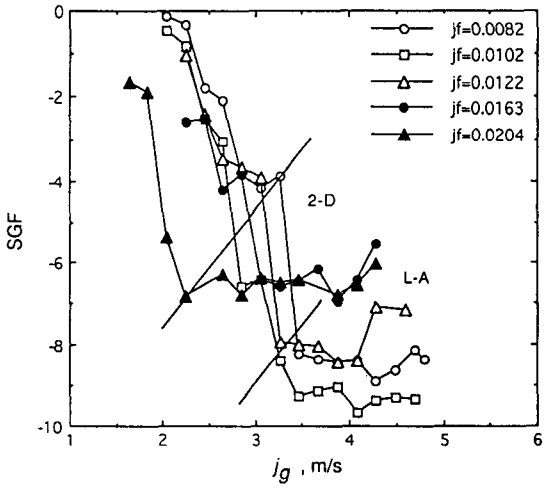

Fig. 10. Variation of Spatial Growth Factor for Higher Range of j_f

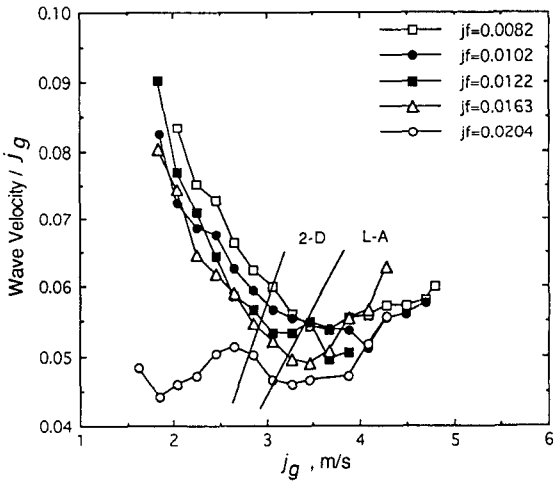

Fig. 12. Effect of j_g on Wave Velocity for Higher Range of j_f

speed camera.

The wave velocities normalized by air superficial velocities are shown in Figs. 11 and 12 as a function of j_g. As shown in Figs. 11 and 12 the dimensionless wave velocity, C/j_g, drastically decreases with j_g in pebbly and 2-D wave regions but the values slightly increase in the large-amplitude wave region. This may be attributed to the coalescence of the large amplitude waves forming an even larger accelerating wave with increasing j_g resulting in a slight increase of C/j_g in a large-amplitude wave region.

The wave lengths are compared in Figs. 13 and 14. For the pebbly and 2-D wave regions, the wave lengths gradually increase but increase sharply in the large-amplitude wave region.

Based on the discussion so far, wave regime map for present study was constructed and is shown in Fig. 15. When comparing the present wave regime map with that of cocurrent flow[Fig. 4 in Ref. 2], it can be noted that all of the wave patterns for present study are located within the smooth-stratified region.

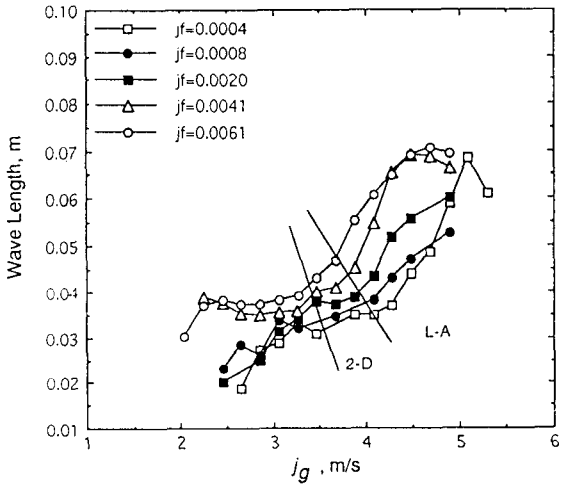

Fig. 13. Variation of Wave Length for Lower Range of j_f

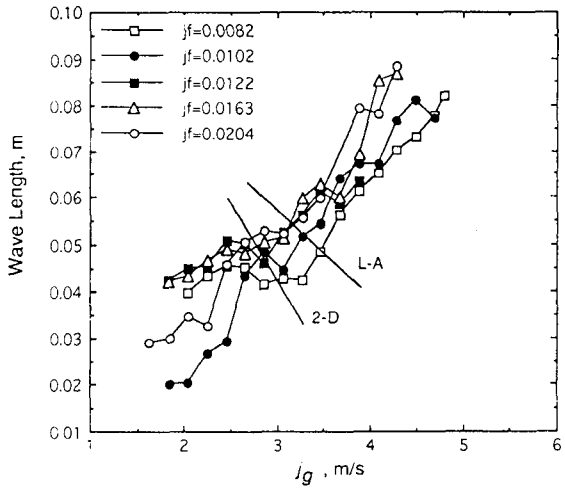

Fig. 14. Variation of Wave Length for Higher Range of j_f

5.3. Interfacial Friction Factor

The empirical correlation for j_g was obtained as $f_g = 0.045\ Re_g^{-0.023}$, for air Reynolds number range between 5×10^3 and 5×10^4[10].

Figure 16 represents f_i as a function of air superficial velocity. As shown in this figure f_i gradually increases until 2-D wave region, but above this region it increases very rapidly. This fact is related to the generation of the large-amplitude waves. This figure also represents that the interfacial friction factor is a strong function of water flow rate in the large-amplitude region.

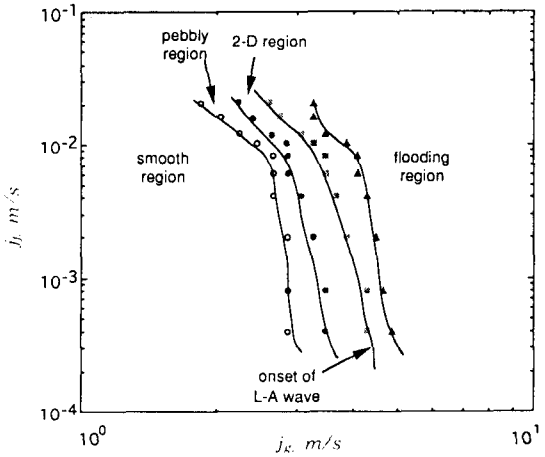

Fig. 15. Flow Regime Map for Present Study

Figure 17 shows that the primary factor affecting f_i/f_g is the air superficial velocity. It can be noted that the relationship between f_i/f_g and j_g is approximately linear until 2-D wave region, but beyond this region the slope indicating the increasing rate is changed greatly owing to the large-amplitude waves. Another feature from this figure is that the values of f_i/f_g for the countercurrent flow are very higher than those of the cocurrent flow predicted by Andritsos and Hanratty [1].

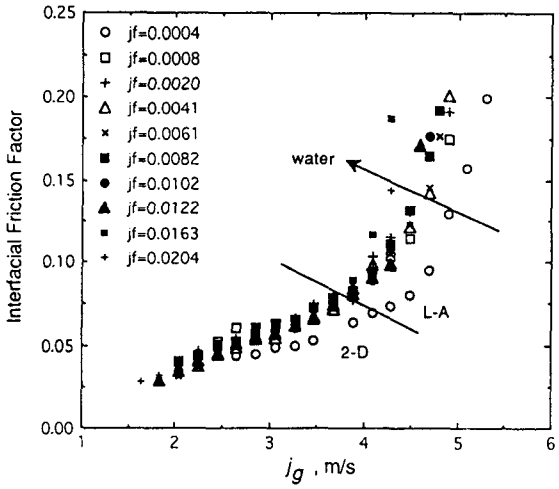

Fig. 16. Interfacial Friction Factor as a Function of j_g

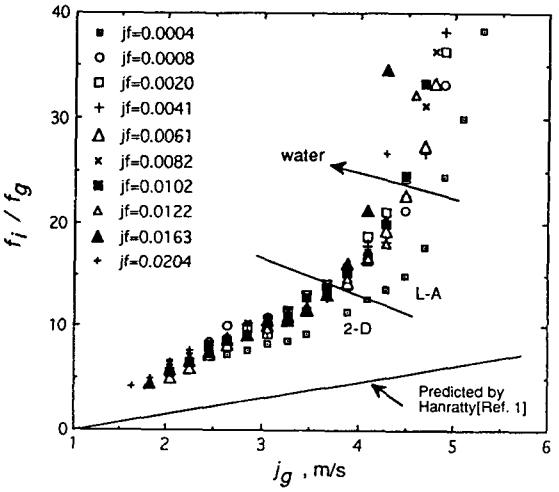

Fig. 17. Effect of Air Superficial Velocity on Interfacial Friction Factor

Experimental uncertainties in the measured quantities are evaluated for the typical case of $j_f=0.0004$ and $j_g=4.487$m/s according to ANSI/ASME PTC 19.1 Code [13]. Accuracy of each instrument is used as a Bias error and the Precision error is evaluated from the standard deviation of the each measued parameter. Uncertainties of j_g and j_f are 4 and 5%, respectively. And the uncertainties of f_i and water thickness are 3.5 and 6%, respectively.

6. Conclusions

On the bases of experiments and ststistical analysis the following conclusions can be derived :

1) The wave patterns observed are a smooth, pebbly, 2-D, large-amplitude, and flooding region.
2) From the high speed video imaging, the large-amplitude waves which carry a larger mass are formed from two modes ; continued growth of 2-D waves and coalescence of 2-D waves.
3) The transition boundaries can be verified by the different nature of ststistical parameters. Especially, the variation of SGF is physically consistent with the onset of the large-amplitude waves.
4) As the waves grow the interfacial friction factor increases linearly with j_g in pebbly and 2-D wave regions. However, it increases drastically in the large-amplitude wave region.

Nomenclature

A flow area, m^2
C wave velocity, m/s
D diameter, m
f friction factor, dimensionless
j superficial velocity, m/s
L length of channel, m
ΔP pressure drop, kPa
S perimeter, m
t time, s

V velocity, m/s
v perturbation
z axis
Δz distance between probes, m

Greek Symbols

ρ density, kg/m^3
i imaginary number
ν viscosity, m^2/s
λ wave length, m

Subscripts

f liquid phase
g gas phase
i interface
k index to denote kth
o reference value
w wall condition

References

1. N. Andritsos and T.J. Hanratty, Influence of Interfacial Waves in Stratified Gas-Liquid Flows, *AIChE J.*, **33,** 444 (1987)
2. P.Y. Lin and T.J. Hanratty, Effect of Pipe Diameter on Flow Patterns for Air-Water Flow in Horizontal Pipes, *Int. J. Multiphase Flow,* **13,** 549 (1987)
3. C.A. Peng, L.A. Jurman and M.J. McCready, Formation of Solitary Waves on Gas-Sheared Liquid Layers, *Int. J. Multiphase Flow,* **17,** 767 (1991)
4. A.E. Dukler, The Role of Waves in Two Phase Flow : Some New Understandings, *Chem. Eng. Education,* **11,** 108 (1977)
5. A.S. Telles and A.E. Dukler, Statistical Characteristics of Thin, Vertical, Wavy, Liquid Films, *Ind. Eng. Chem. Fund.,* **9,** 412 (1970)
6. K.J. Chu and A.E. Dukler, Statistical Characteristics of Thin, Vertical, Wavy Films : part II. Studies of Substrate and Its Wave Structure, *AIChE J.,* **20,** 695 (1974)
7. G.B. Wallis and J. E. Dobson, The Onset of Slugging in Horizontal Stratified Air-Water Flow, *Int. J. Multiphase Flow,* **1,** 173 (1973)
8. G.C. Gardner, Flooded Countercurrent Two-Phase Flow in Horizontal Tubes and Channels, *Int. J. Multiphase Flow,* **9,** 367 (1983)
9. J.E. Koskie, I. Mudawar and W.G. Tiederman, Parallel-Wire Probes for Measurement of Thick Liquid Films, *Int. J. Multiphase Flow,* **15,** 521 (1989)
10. H.J. Chung, *An Experimental Study of Solitary Wave Transition Characteristics for Countercurrent Stratified Air-Water Flows in a Horizontal Pipe,* M.S. Thesis, KAIST (1995)
11. J.S. Bendat and A.G. Piersol, *Random Data Analysis and Measurement Procedures,* John Wiley & Sons, New York (1991)
12. Y. Taitel and A.E. Dukler, A Theoretical Approach to the Lockhart-Martinelli Correlation for Stratified flow, *Int. J. Multiphase Flow,* **2,** 591 (1976)
13. ANSI/ASME PTC 19.1, "ASME Performance Test Codes : Supplement on Instruments and Apparatus, Part-1 ; Measurement Uncertainty"(1985)